Microwave Nondestructive Testing Using an Array of **Near-Field Sensors**

Yuki Gao, Reza K. Amineh, and Maryam Ravan

Applied Electromagnetics Research Lab, New York Institute of Technology, New York, USA (ygao21@nyit.edu)

Abstract— Microwave imaging has been a popular high resolution, non-invasive, and non-contact nondestructive testing (NDT) method for detecting defects and objects in non-metallic media with applications toward testing dielectric slabs, printed circuit board testing, biomedical diagnosis, etc. In this paper, we employ an array of microwave sensors designed based on the complementary split ring resonators (CSRR) along with nearfield holographic microwave imaging (NH-MWI) to assess the hidden features in the dielectric media. In this array, each element resonates at a different frequency in the range of 1 GHz to 10 GHz. Performance of the proposed method is demonstrated via simulation and experimental results.

I. INTRODUCTION

Non-metallic and dielectric materials are in high demands throughout various industries due to benefits such as low-cost, lightweight, durability, and more. It is critical to detect these defects or certain features in these components to avoid undesired events. To address this need, microwave imaging and sensing for dielectric components has been a popular nondestructive testing (NDT) method among all due to promising results [1].

Different configurations of microwave sensors such as spiral resonator sensor [2], split-ring resonator sensor [3], and complementary split ring resonator (CSRR) sensors [4] have been utilized in microwave imaging and sensing. However, the previous works lack advanced post-processing which could lead to more precise assessments. High-resolution nearfield holographic microwave imaging (NH-MWI) results have been presented in [5][6] demonstrating satisfactory performance for NDT applications.

Here, we propose the utilization of an array of sensors resonating from 1 GHz to 10 GHz for evaluating the features in the dielectric media. This sensor array has been adapted from [7]. For the first time, we are utilizing the responses obtained from the multi-frequency near-field sensors and NH-MWI for enhancing the images obtained from near-field sensors.

II. THEORY

Here, we briefly present the theory of NH-MWI for a multi-frequency near-field sensor. Fig. 1 illustrates the imaging setup that includes the sensor that collects backscattered data over a rectangular aperture. The data acquisition and image reconstruction are performed over flat surfaces (along x and y axes) at various z-planes. Besides, the complex-valued scattered field is recorded by the sensor at each position (x, y). Such scattered responses are acquired from subtracting the responses without the presence of the objects from the responses with the objects. The image

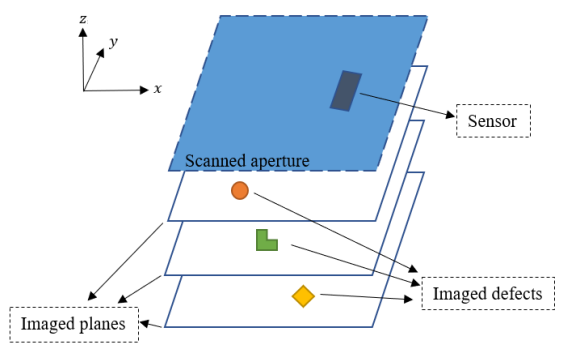


Figure 1. Illustration of the proposed near-field microwave holographic imaging setup.

reconstruction process then provides images over z = z_i planes, where $i = 1, ..., N_z$. Then, the complex-valued scattered field, $E^{SC}(x,y)$, is measured at each sampling position, at N_{ω} frequencies within the band of ω_1 to $\omega_{N_{\omega}}$, by the sensor. The distance between the planes is denoted by Δz .

First, the point-spread functions (PSFs) of the imaging system are obtained as discussed in [8]. The PSF for the *i*-th imaged surface is denoted by $E_i^{\text{SC,PO}}(x, y)$.

To reconstruct images in NH-MWI, it has been shown in [8] that the following system of equations (SoEs) has to be solved at each spatial frequency pair $\kappa = (k_x, k_y)$:

$$\frac{\tilde{\mathbf{E}}^{SC}}{\mathbf{E}^{SC}} = \tilde{\mathbf{D}}\tilde{\mathbf{E}}$$
 (1)

where

$$\underline{\underline{\tilde{\mathbf{E}}}}^{SC} = \begin{bmatrix} \mathbf{\tilde{E}}^{SC}(\boldsymbol{\kappa}, \omega_1) \\ \vdots \\ \mathbf{\tilde{E}}^{SC}(\boldsymbol{\kappa}, \omega_1) \end{bmatrix}$$
(2)

$$\underline{\tilde{\mathbf{E}}}^{SC} = \begin{bmatrix}
\tilde{\mathbf{E}}^{SC}(\boldsymbol{\kappa}, \omega_{1}) \\
\vdots \\
\tilde{\mathbf{E}}^{SC}(\boldsymbol{\kappa}, \omega_{N_{\omega}})
\end{bmatrix}$$

$$\underline{\tilde{\mathbf{E}}} = \begin{bmatrix}
\tilde{\mathbf{E}}^{SC,PO}(\boldsymbol{\kappa}, \omega_{1}) & \cdots & \tilde{\mathbf{E}}^{SC,PO}_{N_{z}}(\boldsymbol{\kappa}, \omega_{1}) \\
\vdots & \ddots & \vdots \\
\tilde{\mathbf{E}}^{SC,PO}_{1}(\boldsymbol{\kappa}, \omega_{N_{\omega}}) & \cdots & \tilde{\mathbf{E}}^{SC,PO}_{N_{z}}(\boldsymbol{\kappa}, \omega_{N_{\omega}})
\end{bmatrix}$$
(2)

$$\underline{\underline{\tilde{\mathbf{F}}}} = \begin{bmatrix} \tilde{f}_1(\boldsymbol{\kappa}) \\ \vdots \\ \tilde{f}_{N_z}(\boldsymbol{\kappa}) \end{bmatrix}$$
(4)

and $\widetilde{\mathbb{E}}^{SC}(\boldsymbol{\kappa}, \omega_n)$, $\widetilde{\mathbb{E}}_i^{SC,PO}(\boldsymbol{\kappa}, \omega_n)$, and $\tilde{f}_i(\boldsymbol{\kappa})$ are Fourier transforms (FTs) of $E^{SC}(x,y,\omega_n)$, $E_i^{SC,PO}(x,y,\omega_n)$, and $f_i(x,y)$, respectively. After solving all SoEs, the images are reconstructed at each depth and are denoted as $f_i(x, y)$ [8].

Here, we assess the overall thickness (along z axis) of cracks. For this purpose, the normalized images obtained from NH-MWI are processed further to obtain the total thickness of a defect. This is implemented as:

$$T(x,y) = \Delta z \left(\sum_{i=1}^{N_z} \frac{|f_i(x,y)|}{M} \right)$$
 (5)

where M is the maximum of the $|f_i(x, y)|$ for all images.

III. RESULTS

Here, a near-field sensor [7] ranging at multiple frequencies within the range of 1 GHz to 10 GHz is utilized. For simplicity, studies are performed with one dimensional (1D) scanning of the sensor array leading to reconstruction of 1D images.

The simulation studies are performed using FEKO software. Fig. 2 shows a dielectric slab which is scanned with the sensor array at a lift-off distance of 1 mm and it has an overall length of L=200 mm, width of W=20 mm, and height of H=6 mm. The slab has a relative permittivity of 4 and a loss tangent of 0.0001. We aim at evaluating the thickness variation of the slab with 2 mm resolution while it has hidden defects. We consider three cases with depth of defects H_D being 2 mm, 4 mm, and 6 mm. For this purpose, the thickness of the 6 mm-thick slab can be divided into three levels of $z_1=2$ mm, $z_2=4$ mm, and $z_3=6$ mm. We add white Gaussian noise with a signal to noise ratio (SNR) of 20 dB to the responses. 1D scanning of the sensor array is performed from -40 mm to 40 mm, with 81 steps, along the x axis.

After applying NH-MWI and computing the defect thickness as per (5). Fig. 3 shows the estimation of defects' thicknesses and the best estimation is for the smallest defect $(H_D = 2 \text{ mm})$ while the larger defects are underestimated.

Fig. 4 shows the setup that consists of a scanning system. We conduct experiments to detect defects in a piece of wood at depths of 2 mm, 4 mm, and 6 mm. For this purpose, three defects are measured with depths of 2 mm, 4 mm, and 6 mm to serve as PSF data. Each defect has approximately a width of 1 mm along the scanning axis. Here, for the imaged scenario, two defects with depths of 4 mm that are at $x = \pm 10$ mm. Fig. 5 shows the estimated thicknesses of the defects when combining the reconstructed 1D images obtained from NH-MWI as per (5). The estimated depth of the defect is close to the true value of 4 mm.

IV. CONCLUSION

For the first time, post-processing based on the concept of NH-MWI was applied to assess defects in nonmetallic slabs using near-field microwave sensors. Simulation and experimental studies demonstrated the accuracy of the proposed technique. For proof-of-concept, 1D scanning and imaging was presented although the presented theory is for two-dimensional (2D) scenarios. Lastly, more results related to biomedical imaging and PCB testing will be available during the conference presentation.

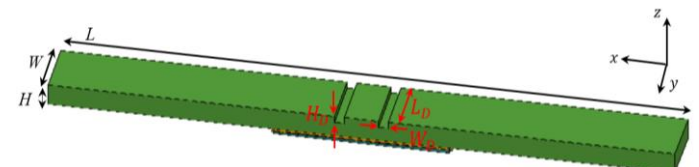


Figure 2. Simulation setup in FEKO.

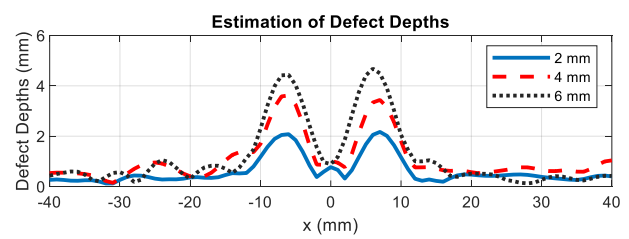


Figure 3. Thickness estimation of defects.

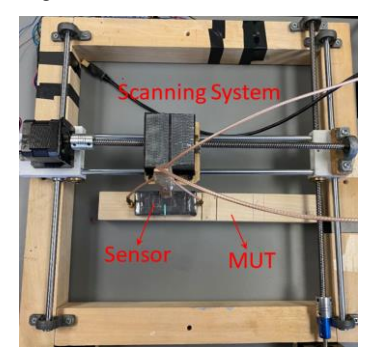


Figure 4. Microwave imaging system.

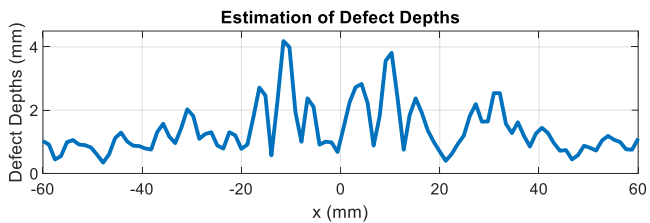


Figure 5. Thickness estimation of defects with depth of 4 mm.

ACKNOWLEDGMENT

This work was supported by the U.S. National Science Foundation (NSF) under Award 1920098.

REFERENCES

- M. T. Ghasr, S. Kharkovsky, R. Zoughi, and R. Austin, "Comparison of near-field millimeter-wave probes for detecting corrosion precursor pitting under paint," *IEEE Trans. Instrum. Meas.*, vol. 54, no. 4, pp. 1497-1504, Aug. 2005.
- [2] K. T. Muhammed Shafi and M. A. Abou-Khousa, "Super-resolution microwave imaging using small loop loaded with spiral resonator," 2017 IEEE SENSORS, 2017, pp. 1-3.
- [3] S. Mukherjee, X. Shi, L. Udpa, S. Udpa, Y. Deng, and P. Chahal, "Design of a split-ring resonator sensor for near-field microwave imaging," *IEEE Sensors Journal*, vol. 18, no. 17, pp. 7066-7076, 1 Sept.1, 2018.
- [4] C.-S. Lee and C.-L. Yang, "Thickness and permittivity measurement in multi-layered dielectric structures using complementary split-ring resonators," *IEEE Sensors Journal*, vol. 14, no. 3, pp. 695-700, March 2014.
- [5] R. K. Amineh, M. Ravan and R. Sharma, "Nondestructive testing of nonmetallic pipes using wideband microwave measurements," *IEEE Trans. Microw. Theory Tech.*, vol. 68, no. 5, pp. 1763-1772, May 2020.
- [6] M. B. Shah, Y. Gao, M. Ravan, and R. K. Amineh, "Quantitative defect size evaluation in fluid-carrying nonmetallic pipes," *IEEE Trans. Microw. Theory Tech.*, vol. 70, no. 8, pp. 4071-4081, Aug. 2022.
- [7] K. Zhang, R. K. Amineh, Z. Dong, and D. Nadler, "Microwave sensing of water quality," *IEEE Access*, vol. 7, pp. 69481-69493, 2019.
- [8] R.K. Amineh, N.K. Nikolova, and M. Ravan, Real-Time Three-Dimensional Imaging of Dielectric Bodies Using Microwave/Millimeter Wave Holography. Wiley & IEEE Press, ISBN: 978-1-119-53886-8, 2019.